AERODYNAMIC INTERFERENCE IN FULL HELICOPTER CONFIGURATIONS AND ASSESSMENT OF NOISE EMISSION: PRE-TEST MODELLING ACTIVITIES FOR THE HELINOVI EXPERIMENTAL CAMPAIGN

Spyros G. Voutsinas	Antonio Visingardi	Jianping Yin	Giles Arnaud
NTUA	CIRA	DLR	Eurocopter SAS
Athens - Greece	Capua – Italy	Braunschweig - Germany	Marseilles - France

Daniele Falchero	Andreas Dummel	Mike Pidd	John Prospathopoulos
Eurocopter SAS	Eurocopter Deutschland	QinetiQ Ltd	NTUA
Marseilles - France	Munich - Germany	Farnborough – UK	Athens - Greece

Abstract

The aerodynamic interference aspects of full helicopter configurations are considered with regard to assessing the potential for noise reduction. The investigation is based on pre-test results from numerical tools of varying complexity and code-to-code comparisons over a range of different flight conditions chosen to match anticipated wind tunnel tests in the DNW on the BO105 scaled model. This work aims at evaluating the different codes as well as at defining the appropriate context for code-to-test comparison. The main bulk of results concern this pre-test activity while some selective comparisons of post-test simulations with measurements support the discussion and conclusions of this exercise.

Introduction

Aerodynamic interference plays an important role in full helicopter configurations. The proximity of the main and tail rotor systems, the immersion of the tail rotor in the main rotor wake, the strong BVI on both the main and tail rotors due to extreme yaw misalignment and finally the interference with the fuselage and the tail boom constitutes the mixture of complex aerodynamic interactions involved in all helicopter flight conditions. The consequences of such interactions are expected to affect noise emissions and excite vibrations. In particular as regards noise, there is a two way connection with aerodynamic interference: the dynamic response of the blade structure to the unsteady aerodynamic loads will change the defining parameters of both the monopole and dipole acoustic sources, while local pressure perturbations resulting from BVI or close body-to-body interactions will affect the dipole acoustic sources. As a whole, the modelling of all these mechanisms defines a challenging modelling task which only recently computational tools have been able to tackle.

In this context and with a view to assessing the current prediction capabilities available in Europe, a co-operative modelling task has been defined within the framework of the HeliNoVi EU project, Ref 1. This task on noise emissions consists of three consecutive activities: the pre-test activity, the validation activity and the assessment of noise reduction potential through configurational and operational changes (See Ref 2 for results on vibrations). The whole activity has been coordinated to closely follow the measurements campaign in the DNW carried out on a 1:2.5 scaled model of the BO105 helicopter, Ref 3. The present paper's main focus is on the pre-test modelling activity which has been concluded. Furthermore through selective comparisons with measurements, Ref 4, the current paper assesses the predictive capabilities of the current state of art computational tools and discusses the points that need further consideration in the two forthcoming phases of the HeliNoVi modelling activities.

Modelling aspects

Modelling assumptions

The problem under consideration in its complete and general definition concerns the analysis of the aeromechanical behaviour of a full helicopter configuration. Its formulation includes: the flight mechanics, the dynamics and the aerodynamics. With reference to the wind tunnel tests against which predictions are to be compared, the following assumptions are introduced:

a) The fuselage is assumed rigid, which is true for the main body of the fuselage but not completely for the tail boom.
b) The attachment of the model on the sting is assumed fixed and rigid. This allows skipping the flight mechanics part by monitoring the loads at the hub during the tests. However the measurements have revealed that this is not always true. At low wind tunnel speeds, the sting vibrated as a

result of its immersion in the free shear layer of the tunnel nozzle.

c) The hub including the control system as well as the drive train for both the main and tail rotors is assumed stiff. This assumption is unavoidable due to the lack of the detailed information needed in order to set up the corresponding dynamic model.

In addition to the above assumptions and with a view to obtaining comparable predictions amongst the various models, it has been decided to exclude the flexibility of the blades during the pre-test calculations. In this case the pitch and flapping angles, or the rotor loads for some models, need to be input. They have been obtained from flight mechanics codes.

Modelling requirements

A commonly recognized requirement for proper modelling of the aeromechanical behaviour of helicopter configurations is to have the wake free so as to allow its adaptation to the local flow conditions. In all of the codes participating in this exercise, free-wake modelling is the default option. Part of the free evolution of the wake is its interaction with solid boundaries which most importantly involves BVI. As the fluid particles contained in the wake approach a solid surface, the vorticity they carry will induce a rapidly increasing velocity which will generate abrupt pressure fluctuations. On the blades, such pressure fluctuations will be detected over the leading edge region where the wake first impinges the blade. Then wake vorticity aligns with the solid surface and such pressure shoots will become less pronounced. If a front loaded airfoil shape is used the effect of the BVI will be seen in the pressure distribution as an apparent change of the effective angle of attack which justifies to a certain extent the use of comprehensive models of the lifting line type. This is the case for the BO105 blade. Were the airfoil not front loaded the trajectory of the incoming fluid particles of the wake should be followed and models that include the geometry of the blade would be expected to be more accurate. The latter becomes important when the fuselage is included. In particular as the MR wake moves downstream, it will interact with the tail boom, the fin and the TR blades in a combined way.

As regards vortex-to-solid interaction, and independently of the approximation followed, the time step plays a critical role. During the pre-test modelling activity the effect of the time step has been assessed on isolated rotors indicating that a time step corresponding to a 1^o azimuth increment is necessary especially when BVI is anticipated, Ref 5. In addition the time step will also affect the length scale of the numerically calculated flow as it specifies the spacing of the wake elements (segments, panels or blobs). This spacing should match the disctretization of the blades. So when the time step decreases, the surface grid must be accordingly refined. In the presence of the TR with 5 times higher rotational speed than that of the MR, such a requirement makes the computations prohibitive. As will be discussed, the compromise one is forced to make for the TR makes the accuracy of the TR predictions questionable.

The time step is also important in order to take proper account of BVI when the geometry of the blades is explicitly included in the computations. In order to have a fair tracking of the vorticity evolution during the wake impinging over a blade, the wake pointers (either nodes or blobs) should be allowed to cover the chord length of the blade in at least 4-5 time steps. On the MR, for 1^o azimuth increment per time step, a fluid particle at the tip will need 3.5 steps to cover the chord length. Also of similar character is the interaction between the TR and the tail boom. Again the TR blade must be given an adequate number of time steps to cover the width of tail boom in order to obtain a sufficient account of this interaction. As the time step increases, unrealistic pressure overshoots will appear on the TR.

Another important aspect concerns the compressibility effects which become important over the advancing side for the higher flight speeds. Over a range of $\pm 45^o$ around the 90^o azimuth position of the blade, shock waves will appear which cannot be taken properly into account by simple correction formulas such as Glauert's. In addition the flow is unsteady so if look-up tables are used a dynamic inflow model must be included, in order to account for the Ma dependence of the load hysteresis, In the present exercise an attempt has been made to include compressibility effects through coupling with CFD models with some success.

Finally of special importance is to account for the flexibility of the blades and the dynamics of the control angles which, despite the scale of the model, modulate the aerodynamics of both rotors. The MR bending will generate a plunging motion while torsion together with the pitch variation will change the apparent

incidence. In the post-test modelling activity which is in progress, aeroelastic coupling has been used and the first simulations indicate substantial improvement of the predictions.

Description of the codes

Five codes of varying complexity have been used in producing the pre-test data base of numerical results plus flight mechanics codes for determining the control angles. The main characteristics of the codes are summarized in Table 1.

	Code1	Code2	Code3	Code4	Code5
Flow	Direct BEM	Indirect BEM	Lifting Line	Indirect BEM	Lifting Line
Kutta	pressure	Flow aligning	-	pressure	-
Wake	Panels	Panels	Vortex Filam.	Vortex Blobs	Vortex Filam.
Ma effects	Glauert/ Full Pot.	Glauert	Glauert & local blade thickening	Glauert/ Euler	Glauert/ Full Pot.
Re effects	-	-	-	2D VI	VI
Dynamics	-	-	Yes	Yes	Yes

Table 1: Main Characteristics of the codes

All codes are formulated within the context of potential theory and the associated integral equation methods that can be derived. In this respect Codes1, 2 & 4 are based on variants of the boundary element method (also known as panel method) while Codes 3 & 5 consist of a chain of interconnected modules both having a lifting-line free wake aerodynamic model of the MR and TR systems as their basic component. Code1 uses the direct integral formulation (the flow within the solid bodies is set to stagnation) while Codes 2 & 4 use the indirect formulation of the Hess type. Codes 1 & 4 use the pressure Kutta condition in order to determine the blade loading while in Code 2 the flow at the wake panels in contact with the blade is aligned with the wake surface which is in consistency with the distribution of the dipole distribution over the mean surface of the blade. Compressibility effects are taken into account basically by applying Glauert's correction. In addition, Codes 1 and 5 have the option to use the incompressible baseline flow computation as input to a full potential compressible code while Code 4 uses instead an Euler solver in a section-by-section procedure. The wake is represented in the form of connected vortex filaments except for Code 4 which applies a vortex blob approximation of the wake. Regarding other worth mentioning features of the codes, a) Codes 3, 4 and 5 are capable of performing coupled aeroelastic computations, b) Code 4 has the option to extend vorticity emission over the blade tip and c) Codes 4 & 5 have the option to include viscous effects by means of viscous-inviscid interaction. Finally as regards noise evaluation, all codes are based on the Ffowcs-Williams Hawking's acoustic analogy theory as detailed in Farassat's formulations. In all computations the quadrapole term has been neglected. A detailed description of different codes can be found in Ref 6 and the references cited therein.

Pre-Test Results

The unsteady pressure field has been recorded during the computations on the blades of the two rotors and over the fuselage surface. By appropriate integration, the sectional as well as global loads are obtained. Also from the pressure signals plus the motion of the blades noise can be evaluated as acoustic pressure signals at specific locations corresponding to the microphone positions during the test, as frequency spectra or noise footprints. Besides pressure recordings, the evolution of the tip vortices of both rotors as well as the flow field itself in the tail rotor region has been recorded. The latter has been used in producing vorticity contours so as to evaluate the interaction of the tail rotor blades with the in coming vortices of the main rotor.

The pre-test activity concerned six flight conditions listed in Table 2 while in Table 3 the predictions of the thrust for both rotors are compared to measurements.

ID	Flight Condition	TR definition
1	12° Climb V_∞ = 33 m/s	Airfoil: S102
2	Level fl. V_∞ = 60 m/s	Airfoil: S102
5	6° descent V_∞ = 33 m/s	Airfoil: S102
10	Level flight V_∞ = 60 m/s	Airfoil: S102 Reduced tip speed
13.2		Airfoil: NACA0012 Advancing Side down
13.4		Airfoil: NACA0012 Advancing Side Up (Reverse sense of rotation)

Table 2. Flight conditions selected for the pre-test activity

The column "PreC" corresponds to the loads as obtained by the flight mechanics code. In general there is fair correlation among the results concerning the MR while for the TR the deviation from either the pre-calculated or the measurements is substantial. Specifically on the TR, there are also significant difference between the pre-calculated and the measured

values. Equally high differences are seen also between the codes. Referring to the discussion on the modelling requirements, it is believed that the relatively large time step (which did not give an azimuthal increment less than 2^o for the MR) is to a certain extent responsible for these deviations. Another reason for having big differences is the trim. The TR is hinged and there is pitch flap coupling. The fixing of the pitch motion and prescribing the flap motion, as provided by a flight mechanics code, presents a very strong restriction, on the TR. So the lack of any compensation might lead to significant load modifications especially since the TR blades interact with tail boom. Finally it is also noted that the highest differences appear in cases ID1, 2 and 10 in which pronounced interaction with the MR wake is anticipated.

Main Rotor (MR) thrust CTx10^4 (Mean value/ Range)						
ID	Code1	Code2	Code4	Code5	PreC	Meas.
1	55.54 ± 8.1	58.90 ±1.83			53.15	53.85
2	66.07 ±26.9	59.06 ±6.78	50.28 ±6.13		52.34	52.16
5			52.43 ±12.13		51.04	51.14
10	69.35 25.2	72.76 ±8.18	59.83 ± 7.13		64.45	64.84
13.2				44.38 ±0.68	52.36	52.79
13.4			48.66 ± 5.97	44.38 ±0.68	52.36	52.31

Trail Rotor (TR) thrust CT.10^4 (Mean value± Range)						
ID	Code1	Code2	Code4	Code5	PreC	Meas.
1	85.33 ± 67	103.87± 50.61			88.48	65.14
2	65.33 ±79.3	61.53 ±76.10	94.1 ±96.1		50.73	41.80
5			23.56 ±23.65		25.14	15.86
10	65.17 ± 150.2	77.43 ± 114.7	100.73 ± 107.6		60.61	54.04
13.2				61.04 ±54.6	50.73	39.67
13.4			43.59 ±67.88	57.24 ±69.07	50.73	44.24

Table 3: Thrust on MR and TR

The data base of results produced is voluminous and a detailed presentation would require substantial space. The selection of results presented in the sequel was made to facilitate the understanding of the flow characteristics of the simulations and guide the further improvement of the modelling procedures. In this section the discussion is restricted to code-to-code comparisons as the control angles finally obtained during the wind tunnel tests are significantly different from those used during the pre-test modelling activity

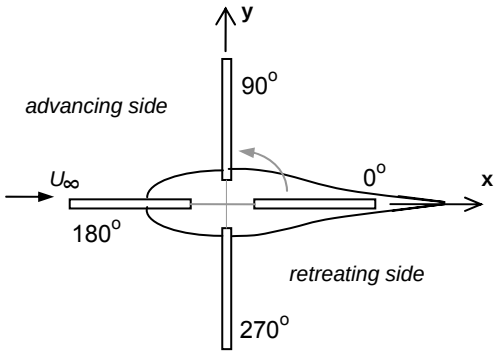

Figure 1: Definitions

ID2: This is a forward flight case at 60m/s so that significant compressibility effects are expected over the advancing side. Five sets of results have been produced two of which correspond to compressible computations. Fig 1 shows the azimuth convention used for presentation of the following figures. Fig 2 gives the normal force coefficient scaled with Ma^2 for the two rotors at three radial stations while in Fig 3 snapshots of the tip vortices lay-out from two simulations are compared.

On the MR and over the 1st quadrant, the various results differ substantially. First the discussion concentrates on the Glauert corrected incompressible results (solid lines). Starting from high loading, Code1 predicts a steep loss followed by an equally quick recovery. This is due to an extensive wake-to-blade interaction clearly seen in Fig 3. On the contrary Codes 2 and 4 predict smooth loading variations over the same range of azimuth angles. Otherwise Code4 predicts consistently lower loading compared to the other two sets of results. Over the next two quadrants, Codes 1 & 4 predictions get closer with Code 4 giving higher values and Code 2 giving a lower loading. Finally over the last quadrant intense wake-to-blade interactions reappear in the Code 1 results, but this time the three codes give comparable levels and trends. It is noted that the downstream half of the rotor disk is an area dominated by the wake evolution which also depends on the flow induced by the fuselage. In all cases the fuselage was modelled as a bluff body without wake, a simplistic approximation resulting in only a displacement effect on the convection of the wake. Commenting on the MR results as a whole, it has been observed that the wake evolution produced by the three codes is

different, so differences in the loading are to be expected. It is difficult to track the mechanisms that can cause such differences. The modelling of the evolution of the wake within the context of vortex methods is a delicate problem. The wake deformation is subjected to a wide range of scales which can result in locally unphysical filament stretching or vorticity intensity changes. In order to suppress such undesired behaviours, the calculation process is filtered. The most commonly used filtering consists of regularizing the velocity calculations by introducing cut-off functions which suppress the singularity in the Biot-Savart integral. However in many cases this is not sufficient so remeshing is required. In the vortex filament method when a vortex segment increases in length above a certain prescribed value, the segment is divided in two. In the vortex blob method remeshing consists of a spatial redistribution of the vorticity contained in the wake through a strength exchange procedure. In simple cases remeshing is computationally affordable. Full helicopter configurations are quite complicated so that inevitably some compromise must be made with a direct impact on the results.

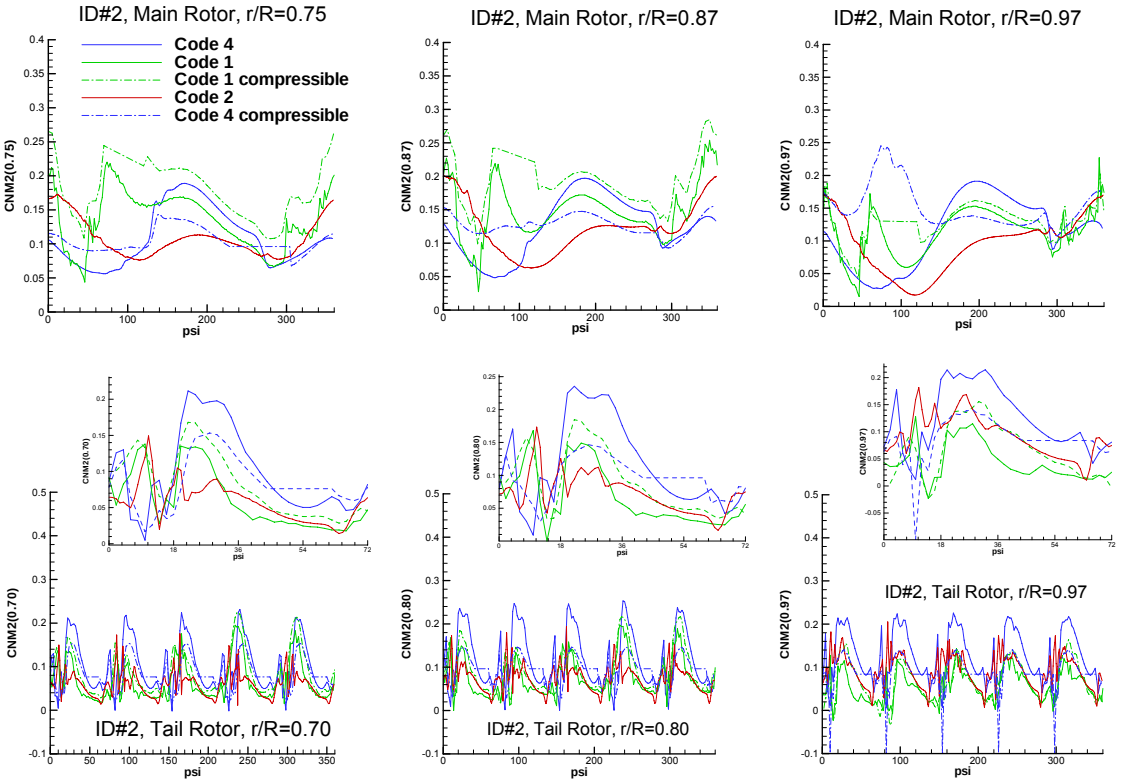

Figure 2: Time evolution of the normal force coefficient $Cn.Ma^2$ at different sections on the two rotors (Case ID#2, forward flight at 60m/s)

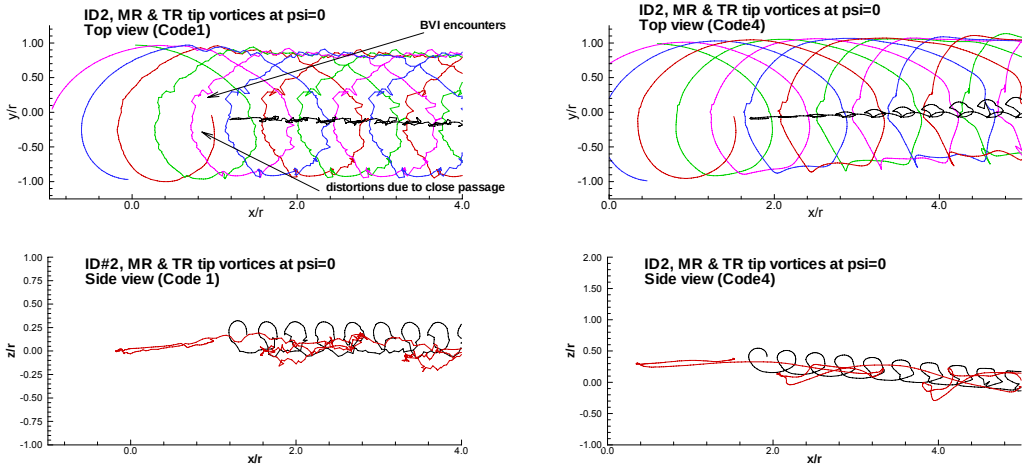

Figure 3: Lay-outs of the tip vortices Case ID#2, forward flight at 60m/s)

On the TR, the results seem more consistent. Codes 1 & 2 indicate similar MRwake-to-TRblade interactions and comparable mean values in accordance with the global loads. Also the higher values given by Code 4 are in accordance with the global loads. On the same plot close ups covering the first TR revolution are also shown. The effect of a highly distorted wake is clearly seen over the first quarter (0º-18º in these plots). Then around 27º the interaction with the tail boom is seen. The boom influence is expected to accelerate the in-plane flow and, since this is in the advancing side of the TR blade, the loading is expected to increase. Regarding the compressible results, the two sets of results are quite different. Code 1 obtains higher values as compared to the Glauert corrected incompressible results. In contrast the results of Code 4 show that the introduction of compressibility effects in the calculations rather flattens the normal force coefficient (lowers the high values and increases the lower ones). It is difficult to track the origin of such differences. Firstly the compressible corrections are produced on the basis of the incompressible flow field which in the two cases is different. Secondly the results depend on how these data are used. Code 1 is using the 3D flow field of the CFD code while Code 4 is using the instantaneous flow direction of the flow at each section independently. Furthermore Code 1 is using a full potential approximation while Code 4 employs a 2D Euler code.

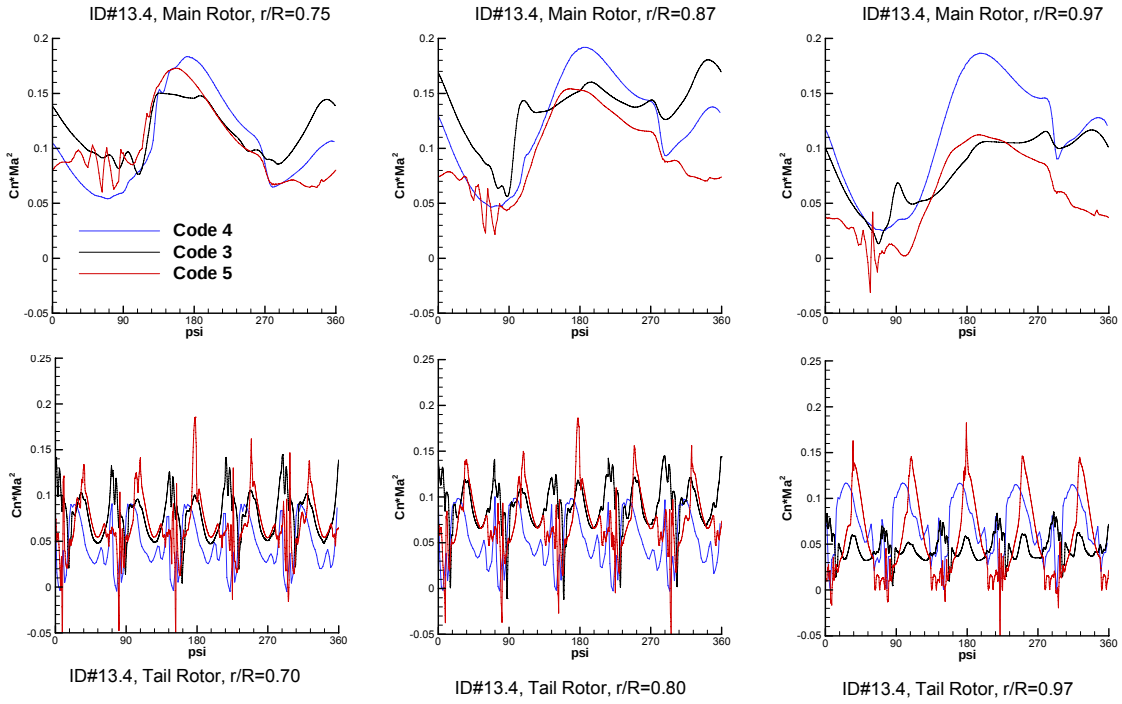

Figure 4: Time evolution of the normal force coefficient Cn.Ma^2 at different sections on the two rotors (Case ID#13.4, forward flight at 60m/s, TR in reverse sense of rotation)

ID13.4: This case is similar to the previous one, except that the TR blade has a different section, but most importantly the sense of rotation is reversed. There is fair agreement over the upwind part of the MR disk except at the tip section where Code 4 predicts higher loading. Over the downwind half of the disk, Code 3 & 4 results agree better. Over the 1st quadrant, Code 5 predicts significant BVI encounters and lower Cn.Ma^2 values contrary to the other two sets of results, possibly due to use of a different predicted trim. Over the last quadrant of the MR disk, the loading distributions are different. Code 3 produces consistently higher values at the inboard sections while at the tip the loading drops and matches the results of Code 4. One possible reason is the special treatment of the blade vorticity at the tip. In Code 3 the tip region is corrected using a semi-empirical model whereas in Code 4 there is tip emission so the peak of the loading is sharp close to the tip. In Code 5 results the loading over the last quadrant exhibits a decreasing trend.

On the TR there are again significant differences. Again Code 4 predicts higher loading at the tip. It is important to notice is an

apparent phase shift in Code 4 results when compared to the other two sets.

ID5: This is a descent flight in which significant BVI encounters are expected. Both sets of results predict intense BVI at the same azimuth locations especially over the retreating side. This can be seen in Figs 5 and 6 where results from Codes 3 & 4 are shown. Code 4 was also run with a refined time step (dashed lines corresponding to 1^{o} azimuth increment) which changed only the intensity of the BVI peaks. In Code 3, time step is variable and the azimuthal step depends on the impulsivity of the interactions and may be less than 0.1°

Over the MR disk area there is good agreement. Further downstream the MR wake interacts with the TR differently. In the Code 3 results the MR wake is trapped by the TR whereas in the Code 4 results this is only partially true. Furthermore over the advancing side Code 4 predicts at the beginning of the first quadrant (~20^{o} of azimuth) an additional encounter at r/R=0.75 which is rather weaker, which is why it is not seen in the wake figures. At the 75% section the behaviour of the normal load over the 1^{st} and 4^{th} quadrant is different in the two sets. Code 3 results show higher loading. At the other two sections the results compare better although again over the last 20^{o} of the cycle at r/R=0.87 the Code 3

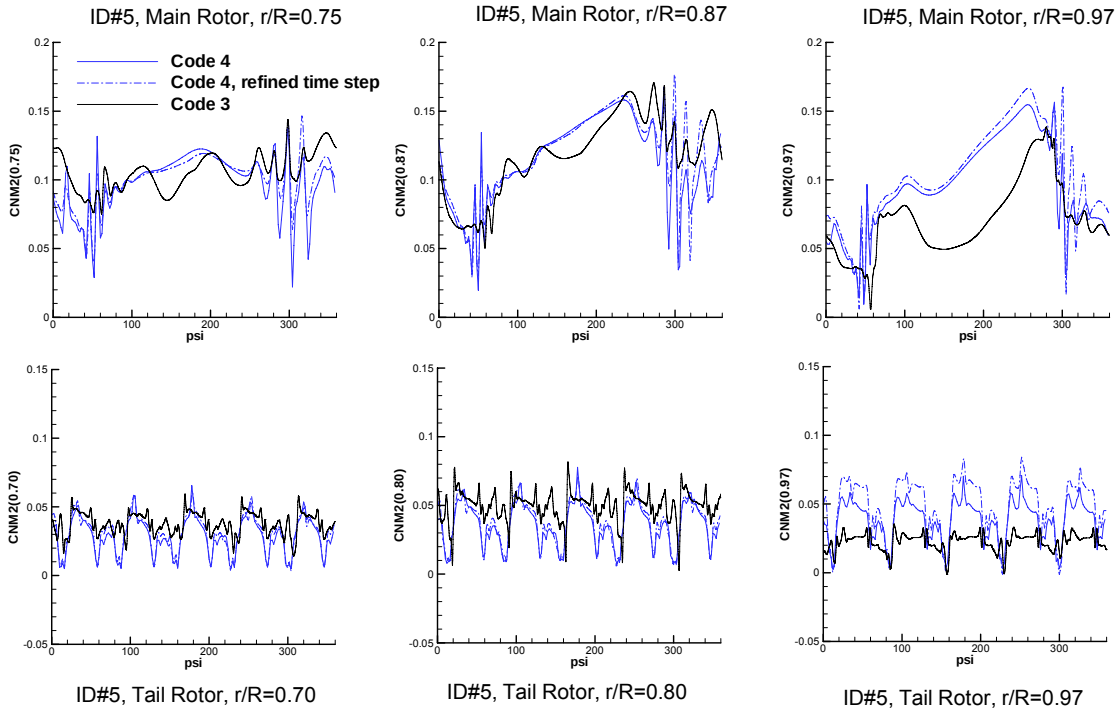

Figure 5: Time evolution of the normal force coefficient $Cn.Ma^{2}$ at different sections on the two rotors (Case ID#5 descent flight at 6^{0} and 33m/s)

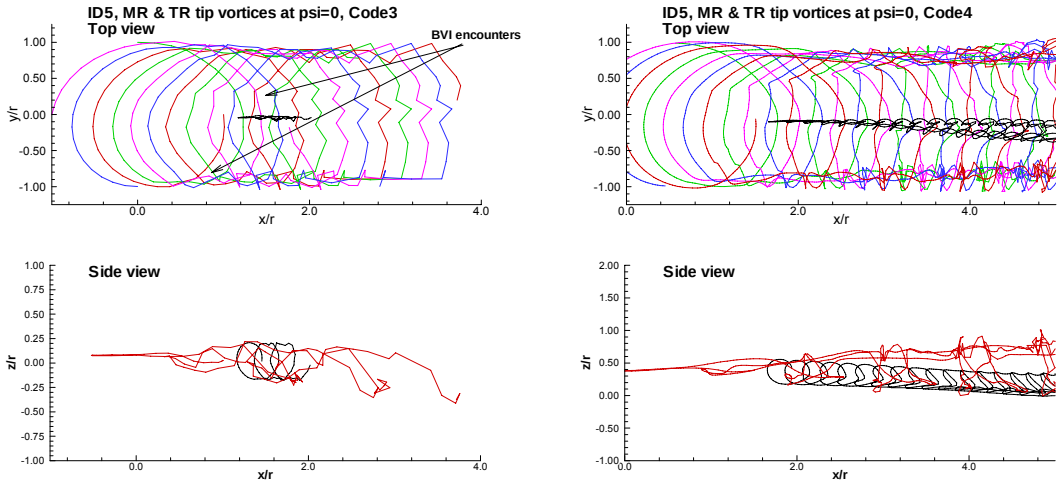

Figure 6: Lay-outs of the tip vortices Case ID#5, descent flight at 6^{0} and 33m/s)

results exhibit a high peak. Also in Code 3 results, the 1st quadrant is followed by an oscillatory variation not shown in the Code 4 results.

Finally at r/R=0.97 there is significant loss of loading in the Code 3 results. One possible reason is the special treatment of the blade vorticity at the tip (See comments on ID13.4).

On the TR, the differences increase as the spanwise location moves from 70% to 97%. At 70% and 87% the sectional loads variations are similar both in form and value, whereas at 97% not only the amplitude but also the mean value in the Code 3 results decrease considerably leading to substantial lower levels when compared to other calculation.

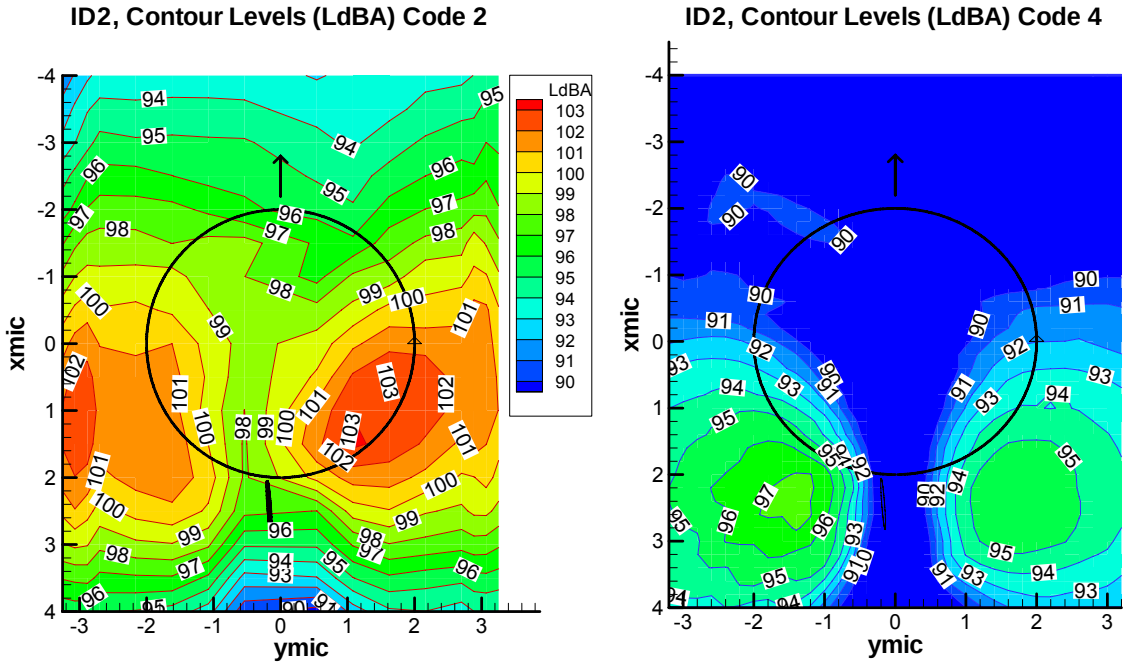

Figure 7: Noise contours (Case ID2, forward flight, 60m/s)

Having in mind that one of the objectives of this exercise is to assess the potential of noise reduction noise, contour plots are now presented and discussed.

ID2: Codes 2 & 4 noise contours are similar (Fig 7). The TR contribution seems to dominate. There is a horizontal shift of the footprint between the two results as well as a difference in the maximum value (103dBA for Code 2 and 97dBA for Code 4). Another difference is that the maximum noise area in the Code 2 results is over the advancing side whereas the opposite is true for the other set of results. It should be remembered that the TR loading, as predicted by Code 4, is higher. This is an indication of the origin of this difference.

ID5: The two results are similar (Fig 8). In addition they agree in the maximum level (~108dBA in both cases) as well as in the locations of the areas of increased noise levels. However they present two differences: the high noise area (advancing side of the MR) in the Code 4 results is more concentrated and restricted within the limits of the MR disk as compared to Code 3 results. This could be due to the density of the grid used in these calculations. In contrast the maximum noise area in the TR region in Code 3 results is more concentrated, when compared to the Code 4 results, while the level in Code 4 contours is higher by approximately 2dBA. Furthermore the pressure fluctuations due to BVI over the retreating side of the MR, which are more pronounced in Code 4 results (Fig 5), are clearly reflected in the noise footprint.

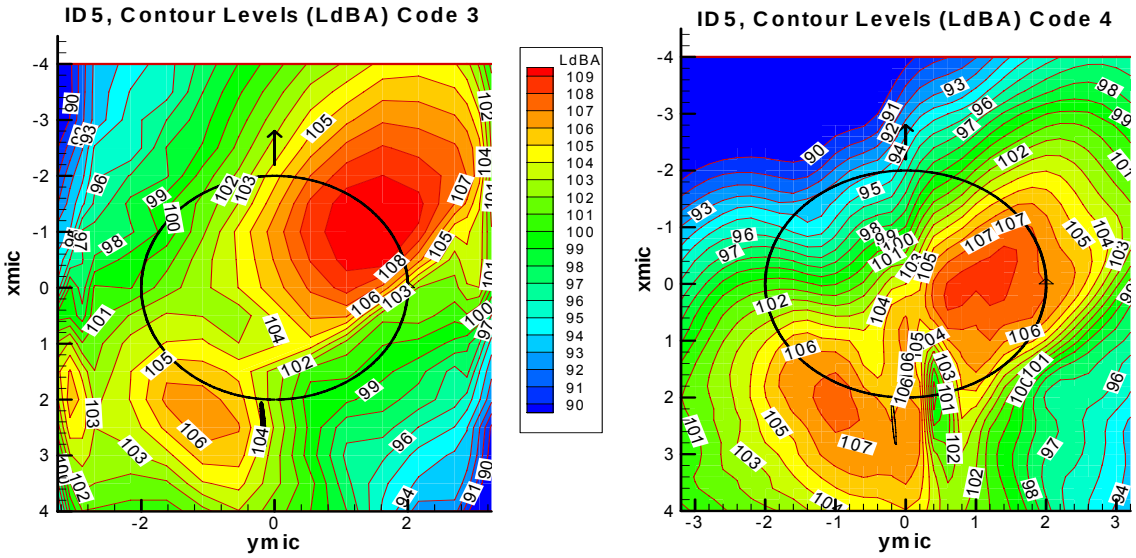

Figure 8: Noise contours (Case ID5, descent flight at 6^0 and 33m/s)

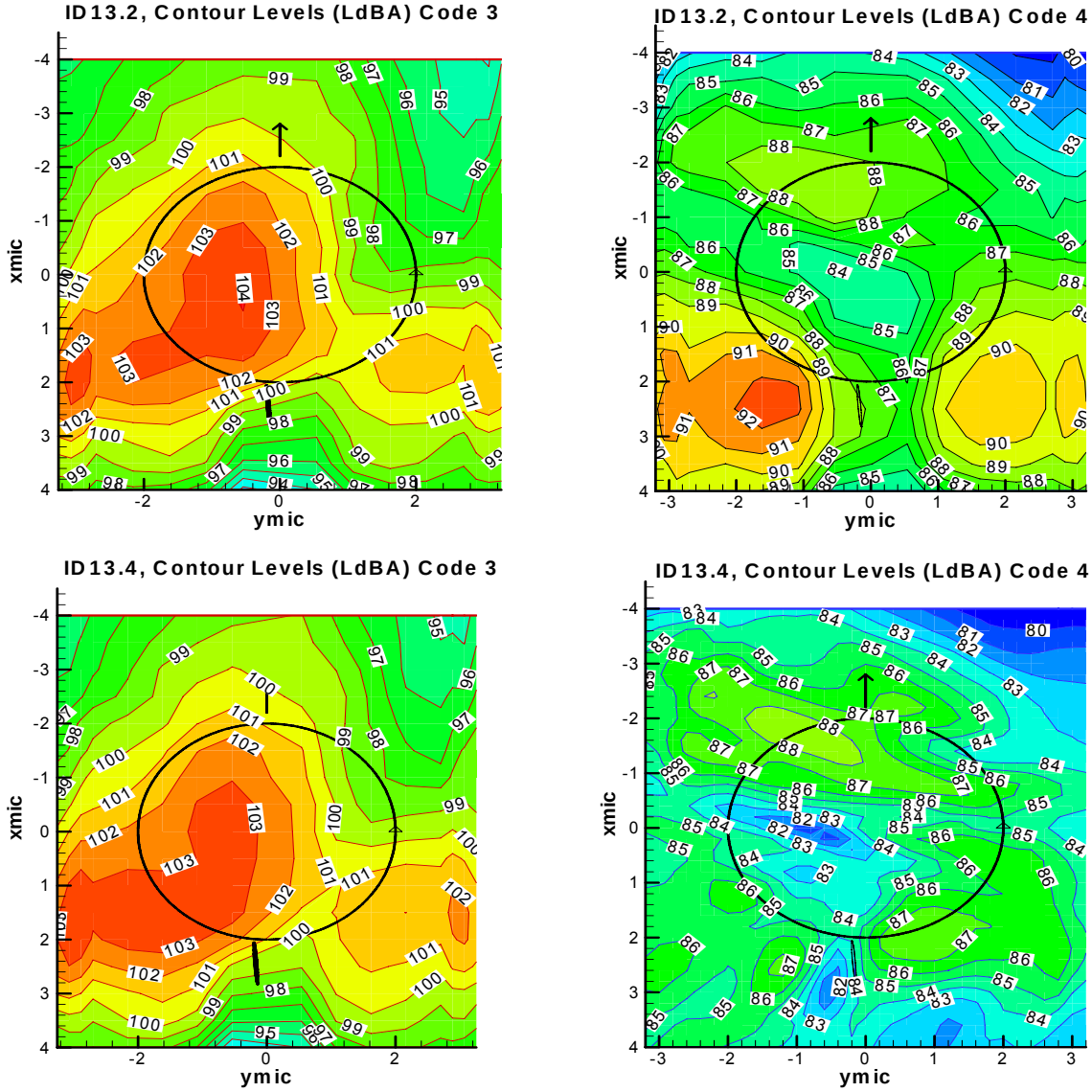

Figure 9: Noise contours for ID13.2 (upper row) & ID13.4 (lower row).

ID13: This is a noise reduction case concerning one possible way to reduce noise, namely the change of the sense of rotation of the TR. In Fig 9 noise footprints are presented for ID13.2 (usual sense of rotation) and ID13.4 (reversed sense of rotation) produced by two different codes. Code 3 results indicate that there is no real difference produced by changing the sense of rotation of the TR, while the results of Code 4 show the opposite. In Code 3 results, noise is dominated by the TR with a load noise area on the right and left parts of the footprint. The extent of the region with high noise levels upstream is due to a combination of the loading noise with the thickness noise (NACA0012 airfoil). Code 4 results for ID13.2 are of similar nature as for ID2 (Fig 7). Again the TR noise is dominant while the maximum level obtained in ID13.2 is similar to that obtained in ID2. By reversing the sense of rotation of the TR, the maximum noise is reduced by ~5dB. Also the high noise area seen in the footprint of ID13.2 is completely eliminated. A possible explanation is the fact that reversing the sense of rotation brings the advancing side of the TR over the upper part of its disk. So the aerodynamic interactions with the MR wake but also with the tail boom do not take place over the unfavorable, as regards noise part of the TR rotation. A similar behavior has been seen in the measurements but further analysis is needed in order to better understand and conclude on the mechanism that generates this change in the noise footprint.

Correlation with measurements

In this section selective comparisons with measurements are discussed. The reason why such comparisons have not been included so far is the significant difference between the pre-test definitions and the real conditions under which the tests were finally conducted. Two forward flight cases at 33m/s (ID4) and 60m/s (ID2) respectively, as well as one descent case (ID5) will be discussed.

Figs 10, 11 and 12 compare post-test predictions with measurements, in terms of the variation of normal force with at the 87% radial station of the MR. Whenever available, pre-test predictions have been added. In the two forward flight cases, the simulations are based on fully coupled aeroelastic computations, while in the descent flight case post-test results have been generated by imposing the measured control angles. When aeroelastic coupling is included, the pitch law is an output

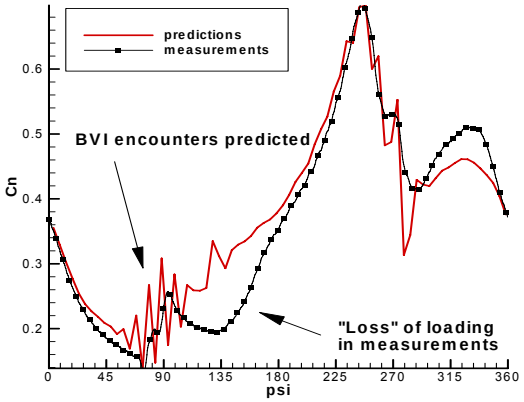

Figure 10: Post test predictions for ID4: Cn time variation at r/R=0.87 of the MR.

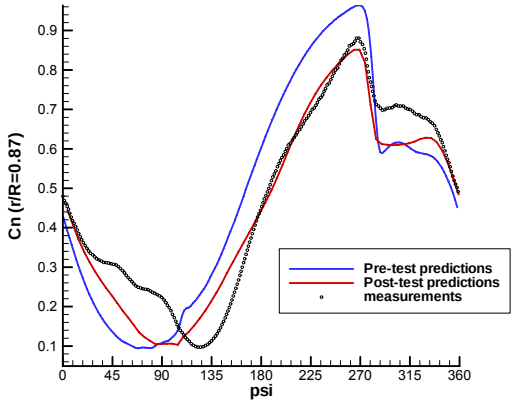

Figure 11: Post test predictions for ID2: Cn time variation at r/R=0.87 of the MR.

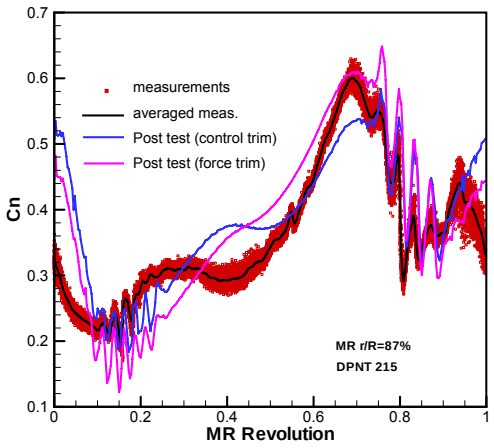

Figure 12: Post test predictions for ID5: Cn time variation at r/R=0.87 of the MR.

of the trimming procedure which matches the loads at the MR and TR hubs according to the measurements. The loads used in this process are the thrust of both rotors and the pitch and roll moments of the MR.The predicted pitch

law of the MR for the two cases compares with the measured ones as follows. In ID4, the collective differed by 0.1°, the cosine component by and 0.3° while the sine component by -0.47°. In ID2 the collective differed by 0.06° while the cyclic components by 0.02° (cosine) and -1.7° (sine). These deviations are clearly reflected in the loading variations. In ID4 there is good correlation over the entire range while in ID2 the difference with the measured data is more pronounced. In this connection it must be noted that the number of pressure sensors over the section does not permit an accurate estimation of the normal force coefficient. As a general comment on these results, there is a clear improvement of the predictions when the aeroelastic coupling is included (Figs 10, 11). By imposing the measured pitch law (Fig 12) and performing aerodynamic calculations there is still improvement but less substantial.

ID4: In this case important compressibility effects are not expected so Glauert's correction formula seems suitable. Commenting on Fig 10 in more detail, a first remark concerns the prediction of BVI over the advancing side of the MR. In the measurements such encounters are weak and can be detected only on the time histories of the pressure over the leading edge. Fig 13 shows the Cp histories at x/c=0.03 on the two sides of the MR blade at three radial stations. The choice of the specific x/c location is important because the BO105 blade is formed by a NACA airfoil which is front loaded so the pressure at the leading edge modulates the overall loading. Predictions indicate that there is an overall wake-to-blade interaction over an extensive part of the rotor disk. It consists of a rather weak interaction as compared to BVI encounters seen in descent flight conditions. In this simulation the fuselage was not included which could be a possible reason for the difference. In the measurements the wake-to-blade interaction besides being weaker as compared to the predictions, is more pronounced at r/R=0.60 and fades further outboard. At the last two radial stations the measurements show a BVI that is localized and more pronounced. In contrast the simulation provides a more diffuse interaction which indicates a different wake evolution. In this connection the processing of the PIV data will be helpful in understanding the flow development in detail. BVI encounters are also predicted over the retreating side. In general predictions compare fairly well with measurements except at the tip section where there is a sharp pressure fluctuation at the 270° azimuth location which is less pronounced in the predictions.

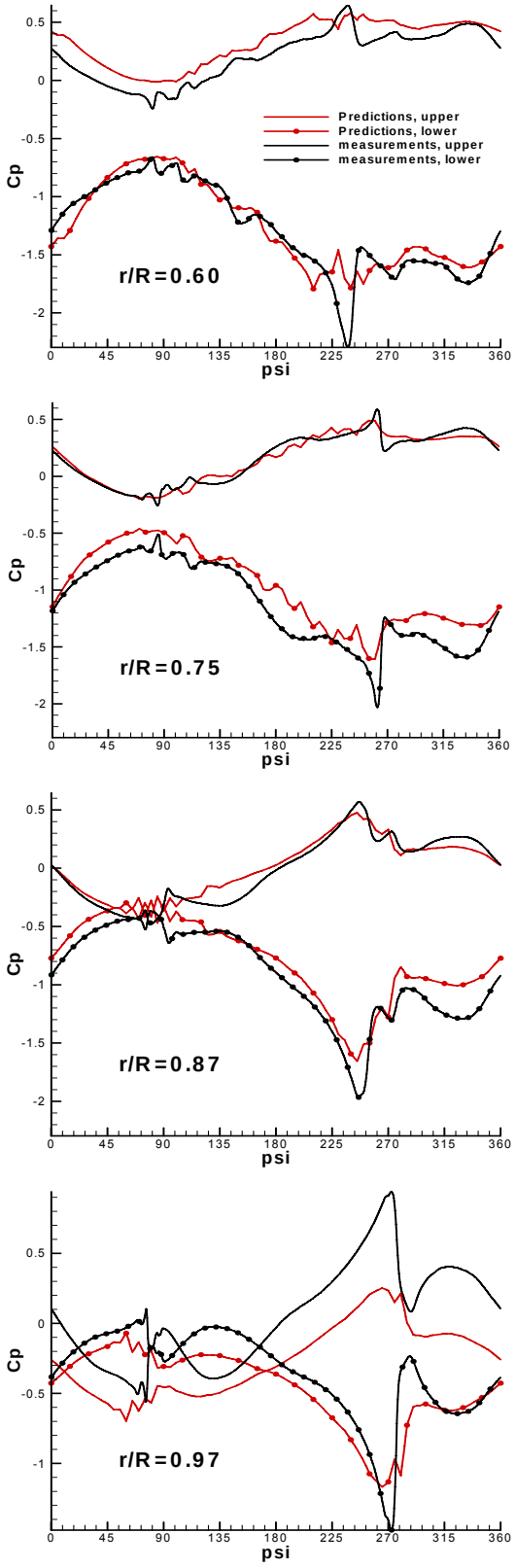

Figure 13: Pressure time histories at x/c=0.03 at different radial stations of the MR blade (ID2, forward flight at 60m/s).

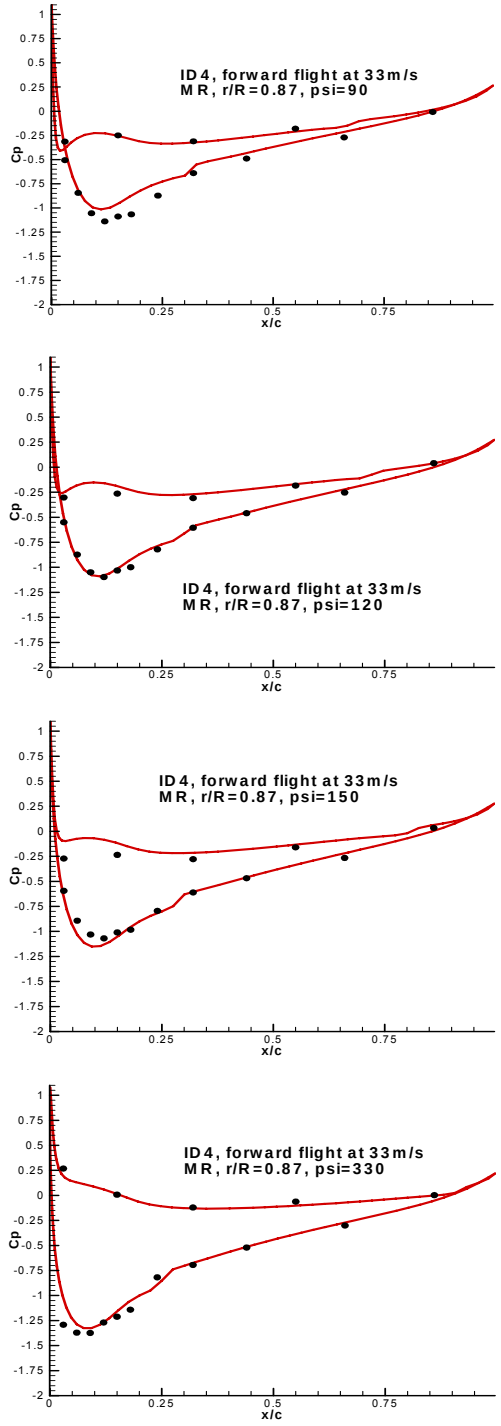

Figure 14: Pressure distributions (ID4 forward flight at 33m/s)

This suggests the presence in the measured flow of more compact tip vortices. In the simulation the compactness of the tip vortex depends strongly on the time step as well as the spanwise resolution of the grid on the blade. A smaller time step will allow a quicker roll-up, while a denser grid over the tip will better simulate the circulation distribution. It is noted that this particular simulation used a time step corresponding to a 5^o of azimuth increment per time step and certainly a smaller step is required.

A second remark concerns the loss of loading in the measurements over the 2^{nd} quadrant. It is not clear what is its origin. Looking at the pressure distributions (Fig14) it is tentatively thought that this is an artefact of the processing on the pressure measurements especially at psi=120^o.

ID2: In this case significant compressibility effects are expected over the advancing side, so the difference in the loading seen in Fig 11 is expected. The deviation from measurements starts at ~20^o of azimuth and fades at ~160^o. In between the predicted variation differs substantially from the measured one. The reason is that the predictions shown in Fig 11 correspond to Glauert corrected calculations. Fig 15 shows the pressure distributions out of which Cn is produced. at azimuth angles of 45^o, 90^o and 120^o (dashed lines). In the same figure solid lines correspond to the compressible calculations. Besides reconfirming that trimming the rotor based on the loads improves the accuracy of the predictions, it is also concluded that compressible calculations are definitely better. Because an Euler code has been used, the shocks are sharp. Moreover the section by section computation neglects the 3D character of the real flow which is seen in the computations as an apparent higher incidence. The use of a 3D Euler is expected to further improve the predictions. It is tempting to suggest the use of the compressible results in the aeroelastic coupling. However besides being computationally prohibitive, the drag force will be certainly wrong while it is doubtful whether the sectional moment, which is in general difficult to predict, will be reliably estimated.

Additional information is provided by the pressure time histories shown in Fig 16. The results concern the x/c=0.03 and 0.06 sectional locations at r/R=0.87 (Fig 16). It is reconfirmed that post-test predictions benefit from a better trim and give more accurate results as compared to the pre-test predictions. Over the advancing side there is good correlation with measurements for the sensors on the pressure side of the section, although over the second quadrant the “loss” of loading seen in the measured Cn variation is clearly marked (on the pressure side). This difference supports the conjecture also made

in discussion of case ID4, that it can be attributed to a different effective angle of attack.

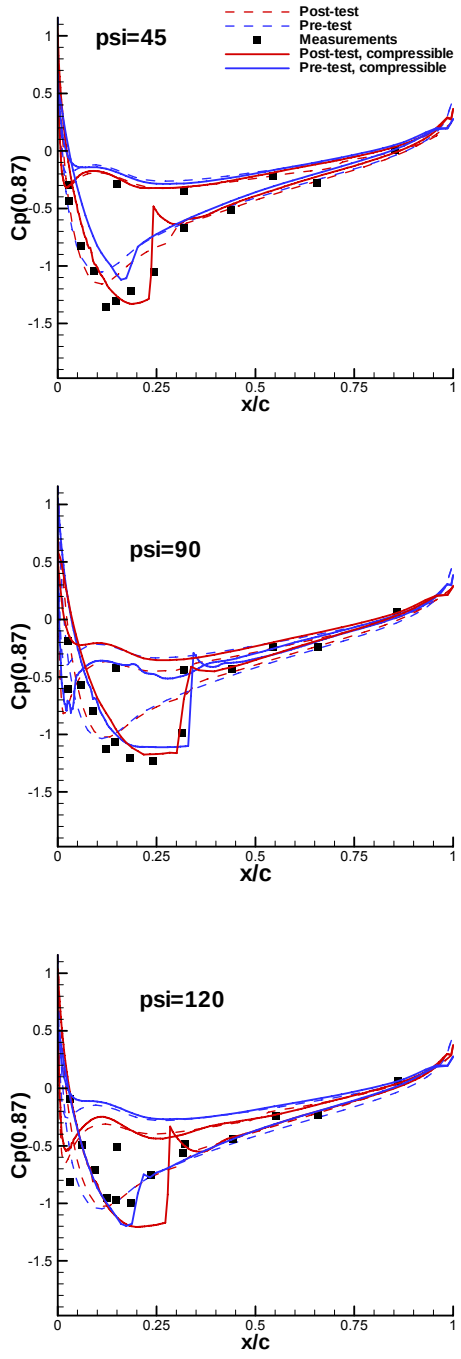

Figure 15: Pressure distributions on the MR at the 87% radial station. Comparison between pre and post test simulations (ID2, forward flight at 60m/s)

Finally in Fig 17, the normal force coefficient on the TR is plotted against measurements for one TR revolution ("psi" still indicates the azimuth of the MR). These plots reconfirm that in order to have meaningful comparisons with measurements it is necessary to trim both rotors in the best possible way. Otherwise, post-test predictions still overestimate the first peak shown in the measurements at the tip.

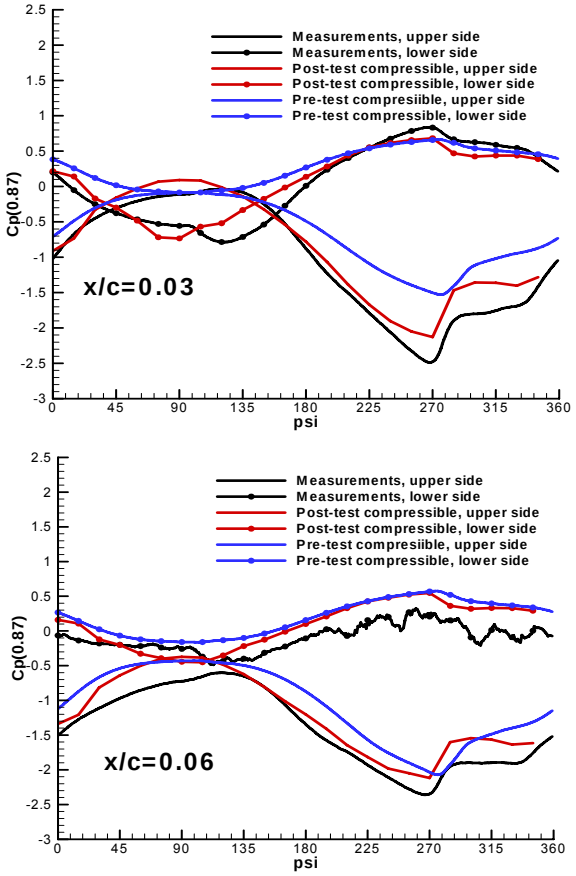

Figure 16: Pressure time histories at x/c=0.03 and 0.06 at r/R=0.87 of the MR blade (ID2, forward flight at 60m/s)

This corresponds to the advancing side of the TR and therefore compressibility effects will be important. The predictions account for Ma dependence through Glauert's correction which in this particular region is not valid.

ID5: In addition to the normal force distribution given in Fig 12, time histories of the pressure at the leading edge at various radial stations are shown in Fig 18. The results correspond to an aeroelastic simulation and concern two different types of trimming: one uses the measured pitch law while the other trims for the loads. A fair correlation is observed. In particular the BVI encounters are well predicted both in terms of position and intensity. Results based on the loads trim compare better especially as regards the suction side. Over the pressure side both sets of predictions are well correlated to measurements. A noticeable deviation over almost the entire rotor disk is clearly seen over the suction side indicates that the loading in

the predictions is consistently lower than the measurements.

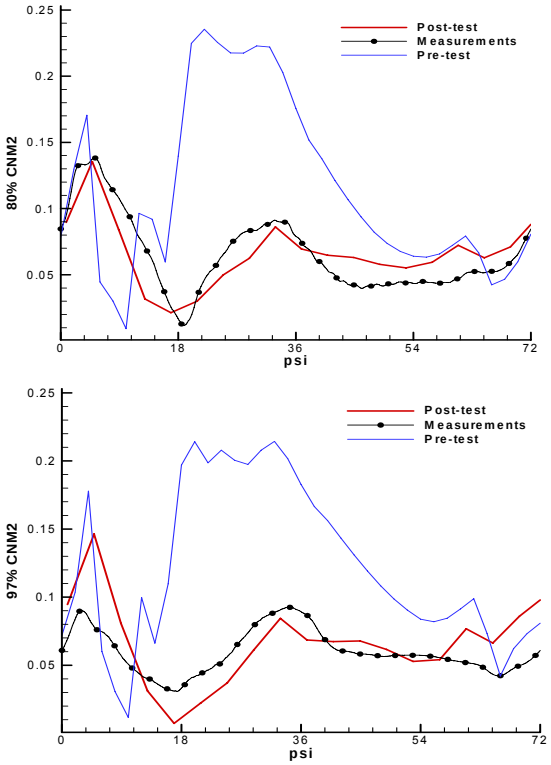

Figure 17: Variation of Cn.Ma^2 at two radial stations of the TR (ID2, forward flight at 60m/s) r/R=0.97.

Finally for the same case post-test predicted noise contours are shown in Fig 19. Again it is reconfirmed that a good correlation with measurements can be obtained when proper trim is provided.

Discussion and Conclusions

A selected collection of pre-test simulations provided by five different codes have been presented. Through code-to-code comparison an evaluation of the prediction capabilities has been carried out. All codes have been able to produce qualitatively the main features of the complex flow around a full helicopter configuration. Quantitative differences have led to a better understanding of the particularities of each method and guidelines for further improvement have been set. The approximation of the wake evolution has emerged as the most important aspect. The second most important point concerns the prediction of the transonic zone which linear theory is unable to tackle. Coupling with compressible CFD provided quite encouraging results. Then as regards noise, consistent results have been produced which is expected since noise computations rely decisively on the aerodynamic predictions. Whenever the aerodynamic results were comparable, this was directly reflected in the noise results.

Post test simulations have been presented. The conclusion of this part is that, in order to obtain comparable results with real flows, it is vital to include the flexibility of the blades. Doing so, predictions were substantially improved. Although the code-to-test comparison phase is still in progress and the processing of the wind tunnel test data has not been completed, it has been possible to understand better the underlying flow mechanisms and set up a framework for a productive final code assessment process. In addition to the necessity of introducing aeroelastic coupling in the simulations and of improving the approximation of the transonic zone through coupling with compressible CFD codes, it became clear that:

- the refinement of the time step at the order of 1^o azimuth increment is important,
- the inclusion of the fuselage especially as regards the TR predictions is important
- the detailed evaluation of the wake evolution through comparisons with PIV pictures is critical for any further improvement of the codes

Post-test noise results were limited so it is not possible to draw conclusions at this stage. However promising comparisons were produced.

Concluding it is believed that a major step towards full aeromechanical simulations of helicopter configurations has been achieved. The HeliNoVi consortium is confident that by concluding the modelling tasks, the helicopter community will be able to utilize simulation codes of high resolution.

Acknowledgement

This work is partly supported by the European Union under the Competitive and Sustainable Growth Programme in the 5th Framework, Contract Nr. G4RD-CT-2001-40113 (HeliNoVi project).

References

1. Langer, H.-J., Dieterich, O., Oerlemans, S., Schneider, O., van der Wall, B., Yin, J. “The EU HeliNoVi Project: Wind Tunnel Investigations for Noise and Vibration Reduction”, Paper 32, 31st European

Rotorcraft Forum, Firenze, Italy, Sept. 13-15, 2005.
2. Dieterich, O., Langer, H.-J., Schneider, O., Imbert, G., Hounjet, M.H.L., Riziotis, V., Carafelli, I., Calvo, R., Clerc, C., Pengel, K. "HeliNoVi: Current Vibration Research Activities", Paper 83, 31st European Rotorcraft Forum, Firenze, Italy, Sept. 13-15, 2005
3. Langer, H.-J., Junker, B., Plassmeier, V., Buchner, F., Mikulla, V., Mercher, E. "The unique capabilities of a complete Mach-scaled Helicopter model for the DNW-LLF", Paper 50, 27th European Rotorcraft Forum, Moscow, 2001
4. Yin, J., Van der Wall, B., Oerlemans, S., et al: Representative Test results from HELINOVI Aeroacoustic Main Rotor/Tail Rotor/Fuselage Test in DNW; Paper 042, 31st European Rotorcraft Forum; FIRENZE, Italy; Sept. 13-15, 2005
5. Voutsinas,S., Yin, J. Triantos, D. "Refinement assessment report" HeliNoVi, Report D1.1-1, 2002.
6. A. Visingardi, Yin, J., Voutsinas, S. "Code_to_Code Comparison on Pre-TestAerodynamic and Aeroacoustic Predictions", HeliNoVi, Report D1.1-3, 2004

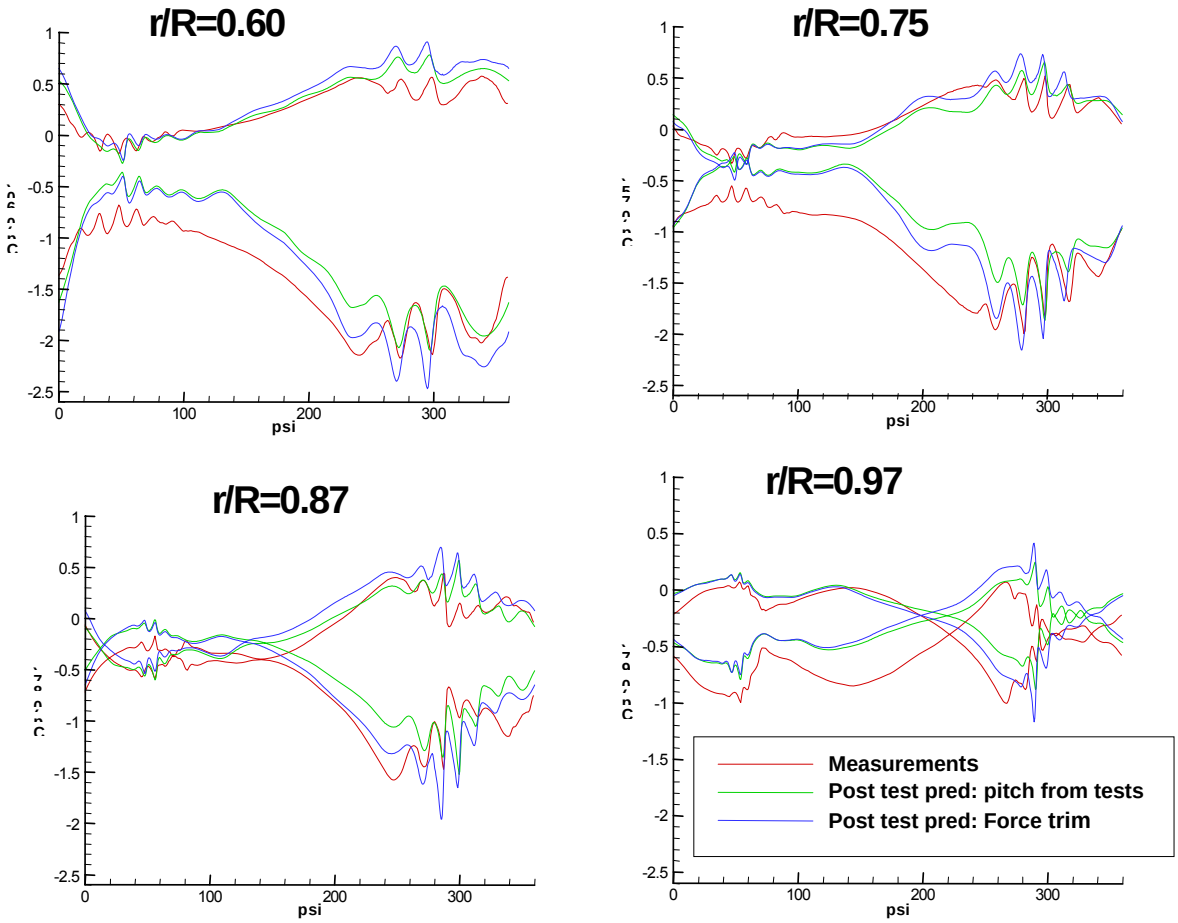

Figure 18: Pressure time histories at x/c=0.03 of different radial stations of the MR blade (ID5, 6° descent flight at 33m/s)

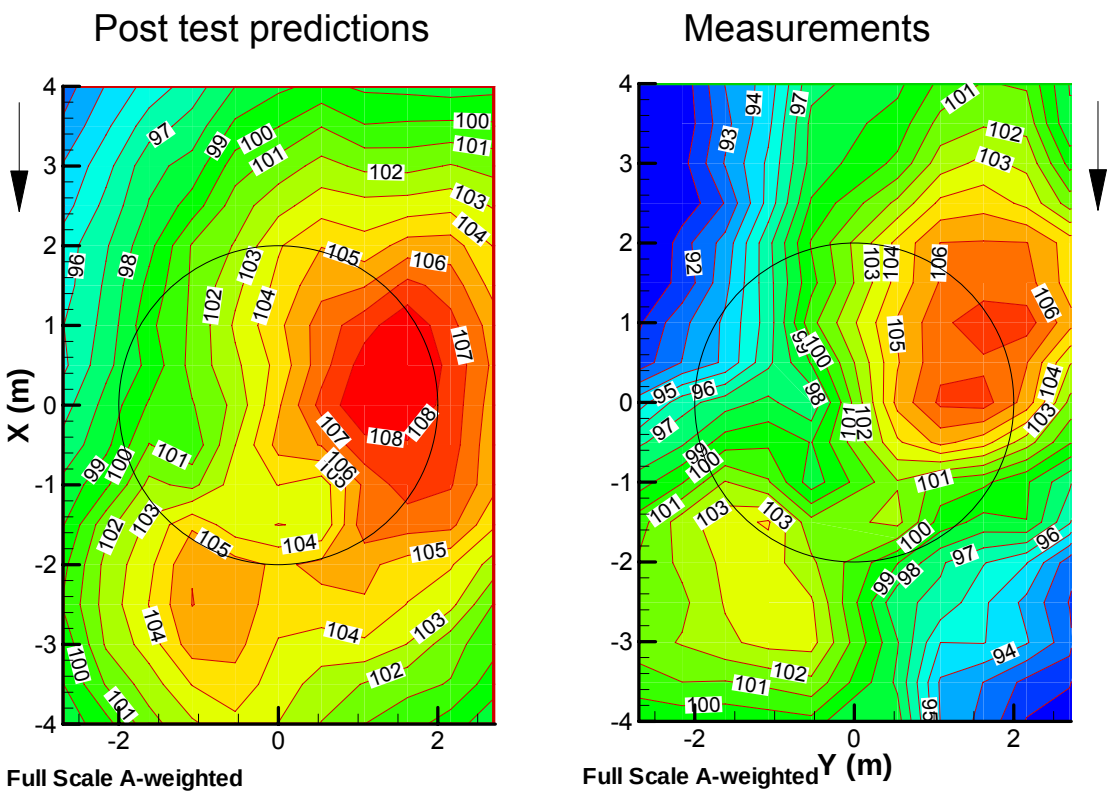

Figure 19: Noise contours (ID5, descent flight): Post test predictions vs measurements